

Sterile Neutrinos: Propagation in Matter and Sensitivity to Sterile Mass Ordering

Dibya S. Chattopadhyay ^a Moon Moon Devi ^b Amol Dighe ^a Debajyoti Dutta ^c
Dipyaman Pramanik ^d Sushant K. Raut ^e

^aTata Institute of Fundamental Research, Homi Bhabha Road, Colaba, Mumbai 400005, India

^bDepartment of Physics, Tezpur University, Assam, 784028, India

^cAssam Don Bosco University, Tapesia Campus, Sonapur, Assam, 782402 India

^dInstituto de Física Gleb Wataghin - UNICAMP, 13083-859, Campinas, São Paulo, Brazil

^eDivision of Sciences, Krea University, Sri City, India 517646

E-mail: d.s.chattopadhyay@theory.tifr.res.in, devimm@tezu.ernet.in,
amol@theory.tifr.res.in, debajyoti.dutta@dbuniversity.ac.in,
dpramanik92@gmail.com, sushant.raut@krea.edu.in

ABSTRACT: We analytically calculate the neutrino conversion probability $P_{\mu e}$ in the presence of sterile neutrinos, with exact dependence on Δm_{41}^2 and with matter effects explicitly included. Using perturbative expansion in small parameters, the terms involving the small mixing angles θ_{24} and θ_{34} can be separated out, with θ_{34} dependence only arising due to matter effects. We express $P_{\mu e}$ in terms of the quantities of the form $\sin(x)/x$, which helps in elucidating its dependence on matter effects and a wide range of Δm_{41}^2 values. Our analytic expressions allow us to predict the effects of the sign of Δm_{41}^2 at a long baseline experiment like DUNE. We numerically calculate the sensitivity of DUNE to the sterile mass ordering and find that this sensitivity can be significant in the range $|\Delta m_{41}^2| \sim (10^{-4} - 10^{-2}) \text{ eV}^2$, for either mass ordering of active neutrinos. The dependence of this sensitivity on the value of Δm_{41}^2 for all mass ordering combinations can be explained by investigating the resonance-like terms appearing due to the interplay between the sterile sector and matter effects.

Contents

1	Introduction	1
2	Analytic Approximation for the Conversion Probability $P_{\mu e}$	4
2.1	Decoupling of θ_{24} and θ_{34} -dependent terms in matter	5
2.2	$P_{\mu e}$ in the $\sin(x)/x$ form, with $A_n = -A_e/2$	6
2.3	Effects of sterile mass ordering on $P_{\mu e}$ at DUNE	7
2.4	Peaks and dips in $P_{\mu e}$ at DUNE due to sterile neutrino	10
3	Sensitivity to sterile mass ordering at DUNE	12
3.1	Analysis procedure	12
3.2	Dependence of the sensitivity on $ \Delta m_{41}^2 $	14
3.3	Dependence of sensitivity on mass ordering combinations	15
3.4	Interplay between Δm_{41}^2 and matter effects	17
4	Conclusions	18

1 Introduction

The phenomenon of neutrino oscillations, originating from different masses of three active neutrinos and mixing among the three neutrino flavors, is now well-established, and explains all the data from solar, atmospheric, and reactor neutrinos quite well [1, 2]. The magnitudes of mass-squared differences $\Delta m_{ij}^2 \equiv m_i^2 - m_j^2$ between each pair of neutrino mass eigenstates, as well as the mixing angles θ_{ij} that parameterize the neutrino mixing matrix, have been measured to an accuracy of better than 10%, and the sign of Δm_{21}^2 has been determined to be positive from the solar neutrino data [3–6]. Two of the parameters controlling neutrino mixing and oscillations that have not been determined so far are the mass ordering, i.e. the sign of Δm_{31}^2 , and the CP-violating phase δ_{13} . Many of the future experiments [7–11] have the measurement of these two quantities as one of their primary aims.

While the data from the collider experiments [12] have ruled out the presence of more than three light neutrinos that undergo weak interactions, the possibility of one or more sterile neutrino species, which do not undergo weak interactions, remains. The existence of a sterile neutrino is a crucial question that connects to our quest for a fundamental theory at the high scale, from which the standard model (SM) of particle physics would emerge as an effective theory. Indeed, even the origin of the masses of active neutrinos themselves needs the introduction of new physics at the high scale [13–17]. Any light fermion in these theories that is a SM gauge singlet can mix with active neutrinos and play the role of a sterile neutrino.

Active mass ordering	Sterile mass ordering	Combination
$\Delta m_{31}^2 > 0$ (N)	$\Delta m_{41}^2 > 0$ (Ns)	N-Ns
	$\Delta m_{41}^2 < 0$ (Is)	N-Is
$\Delta m_{31}^2 < 0$ (I)	$\Delta m_{41}^2 > 0$ (Ns)	I-Ns
	$\Delta m_{41}^2 < 0$ (Is)	I-Is

Table 1. All four possible combinations of active and sterile mass ordering

Some short-baseline accelerator experiments have claimed observations that would need the presence of sterile neutrinos for their explanation [18–22]. There are also indications that the reactor neutrino data may be accounted for better in the presence of sterile neutrinos [20, 23–27]. However, the evidence is still inconclusive and in tension with other experiments [26–32], as well as recent theoretical calculations related to reactor nuclear effects [33]. The short-baseline experiments mentioned above need sterile neutrinos with $\Delta m_{41}^2 \sim 0.1 - 1 \text{ eV}^2$ for explaining the data, where m_4 is the mass of the eigenstate with the largest sterile neutrino component. Short-baseline Gallium radioactive source experiments like GALLEX [34–36], SAGE [37–40] and BEST [41, 42] have measured electron neutrino disappearance levels that are much higher than expected. However, note that the sterile neutrino mixing angles needed to solve such anomalies are in tension [43] with the constraints from other experiments, and may need inclusion of more exotic new physics scenarios [44]. Sterile neutrinos of keV masses have also been proposed as candidates for warm dark matter in theories like the ν SM [45–48]. They could also be useful in understanding the formation of supermassive stars [49, 50]. On the other hand, superlight ($\Delta m_{41}^2 \sim 10^{-5} \text{ eV}^2$) sterile neutrinos [51–55] may be the explanation for the lack of upturn in the spectrum of solar neutrino oscillation probability for energies below $\sim 8 \text{ MeV}$ [56–58]. Recently, it has been pointed out [59] that a sterile neutrino with $\Delta m_{4\ell}^2 \sim 10^{-2} \text{ eV}^2$ (where ℓ is the lightest neutrino) can help resolve the tension between the T2K and NOvA data [3, 5, 6, 60]. The question of whether sterile neutrinos exist, and if they do, what their mass and mixing parameters are, is still quite open.

We restrict our attention to the scenario with one sterile neutrino species. Neutrino oscillation experiments have constrained the mixing angles in the sterile sector ($\theta_{14}, \theta_{24}, \theta_{34}$) over a wide $|\Delta m_{41}^2|$ range [61]. However, the identification of the sign of Δm_{41}^2 itself has not yet been explored in detail. Data from cosmology restrict the total amount of hot dark matter in the Universe and hence constrains the sum of masses of all neutrinos to $\sum m_i \lesssim O(0.1) \text{ eV}$, therefore the sign of Δm_{41}^2 cannot be negative for $|\Delta m_{41}^2| \gtrsim 0.1 \text{ eV}^2$ [2, 62, 63]. However, no such constraint has been obtained for smaller $|\Delta m_{41}^2|$ values. If we were to detect the presence of a sterile neutrino in this mass range, the question of sterile mass ordering — “normal” (Ns) for $\Delta m_{41}^2 > 0$ or “inverted” (Is) for $\Delta m_{41}^2 < 0$ — would still need to be settled. Indeed, since the mass ordering in the active sector (defined by the sign of Δm_{31}^2) as well as the mass ordering in the sterile sector (defined by the sign of Δm_{41}^2) are unknown, we get a total of 4 possible mass ordering combinations as shown in Table 1. The question of mass ordering in the active sector is at the forefront of future physics goals of neutrino experiments. As far as the sterile mass ordering is

concerned, it has been shown [64] that the proposed iron calorimeter (ICAL) experiment at the India-based Neutrino Observatory (INO) [65] will be sensitive to the sign of $|\Delta m_{41}^2|$ if $|\Delta m_{41}^2| \in (10^{-4}, 10^{-2}) \text{ eV}^2$. However, such an analysis in the context of long-baseline experiments has never been carried out.

The neutrino oscillation probabilities in the presence of sterile neutrinos in vacuum have been obtained in [66, 67]. Matter effects are included in analytic or semi analytic approaches, in the scenarios where Δm_{41}^2 is large and hence sterile neutrino oscillations are fast [68–73], and for super-light sterile neutrinos where $\Delta m_{41}^2 \lesssim \Delta m_{21}^2$ [54, 55]. For a wider range of Δm_{41}^2 encompassing heavy as well as light sterile neutrinos, various approaches for calculating neutrino oscillation probabilities have been employed [74–79]. However, to explore the complex dependence of sterile oscillations on neutrino mixing parameters, in the presence of matter, one needs to calculate these probabilities with explicit analytic dependence on Δm_{41}^2 , the matter potential and neutrino mixing parameters.

In this paper, we calculate the conversion probability $P_{\mu e}$ that is valid for all values of Δm_{41}^2 , and has explicit dependence on matter effects. When calculated as an expansion in the small parameters, the dependence on sterile mixing angles θ_{24} and θ_{34} is found to be separable [72]. Moreover, the θ_{34} dependence appears only due to neutral-current forward scattering of neutrinos in matter [66, 67]. Further, expressing the probability as a summation of terms of the $\sin(x)/x$ form allows the identification of regions in the sterile neutrino parameter space where the combined effect of sterile mixing and matter effect is significant. This also enables us to explain the features of sterile contribution to $P_{\mu e}$, such as the positions and heights of dips and peaks of $P_{\mu e}$, at a long-baseline neutrino experiment.

The analytic expressions calculated in this paper facilitate explorations of many aspects of sterile neutrino oscillations in matter for any possible value of Δm_{41}^2 . In this article, we focus on identifying the sterile mass ordering at a long-baseline neutrino experiment, taking the Deep Underground Neutrino Experiment (DUNE) [10, 11, 80] as an example. Our analytic expressions indicate that DUNE would be highly sensitive to the mass ordering in the sterile sector in the range of $|\Delta m_{41}^2| \in (10^{-4}, 10^{-2}) \text{ eV}^2$, where matter effects will play a significant role. We point out key features of sterile neutrino contributions and determine the sensitivity of DUNE to the sign of Δm_{41}^2 . We also study how the current uncertainties in the values of other oscillation parameters would affect this sensitivity. We carry out the analyses for all the four mass ordering combinations in table 1, for both neutrinos and antineutrinos.

In section 2, we present approximate expressions for the neutrino oscillation probability $P_{\mu e}$ in constant density matter in the presence of a sterile neutrino. We analytically explore the sterile mass ordering effects and point out the parameter ranges where these effects will be significant. In section 3, we calculate the sensitivity of DUNE to sterile mass ordering. We also explore the dependence of this sensitivity on $|\Delta m_{41}^2|$ and all four mass ordering combinations. In section 4 we conclude with a discussion on further broader usage of the formalism developed in this paper.

2 Analytic Approximation for the Conversion Probability $P_{\mu e}$

The upcoming long-baseline neutrino experiment DUNE is primarily sensitive to the conversion channel $\nu_\mu \rightarrow \nu_e$. In this section, we calculate the analytic form for the probability $P_{\mu e} \equiv P(\nu_\mu \rightarrow \nu_e)$ in constant density matter, explicitly including the effects of a sterile neutrino of arbitrary mass. Let us first define the Hamiltonian for the $3 + 1$ neutrino system, in the flavor basis:

$$\mathcal{H}_{3+1} = \frac{1}{2E_\nu} U \begin{pmatrix} 0 & 0 & 0 & 0 \\ 0 & \Delta m_{21}^2 & 0 & 0 \\ 0 & 0 & \Delta m_{31}^2 & 0 \\ 0 & 0 & 0 & \Delta m_{41}^2 \end{pmatrix} U^\dagger + \begin{pmatrix} V_e + V_n & 0 & 0 & 0 \\ 0 & V_n & 0 & 0 \\ 0 & 0 & V_n & 0 \\ 0 & 0 & 0 & 0 \end{pmatrix}. \quad (2.1)$$

In the above equation, $V_e \equiv \sqrt{2}G_F N_e$ and $V_n \equiv -G_F N_n/\sqrt{2}$ are the effective charged-current and neutral-current potentials, respectively, experienced by neutrinos due to matter effects. Here, G_F is the Fermi constant and N_e (N_n) is electron (neutron) density. The unitary rotation matrix U is parametrized as $U = U_{34} U_{24} U_{14} U_{23} U_{13} U_{12}$, where each U_{ij} matrix is the unitary rotation matrix in ij -plane. The matrix U is expressed in terms of 6 independent rotation angles ($\theta_{12}, \theta_{13}, \theta_{23}, \theta_{14}, \theta_{24}, \theta_{34}$) and 3 independent phases ($\delta_{13}, \delta_{24}, \delta_{34}$).

We define a few dimensionless quantities that will be used frequently in the analysis:

$$\alpha \equiv \frac{\Delta m_{21}^2}{\Delta m_{31}^2}, \quad R \equiv \frac{\Delta m_{41}^2}{\Delta m_{31}^2}, \quad A_e \equiv \frac{2E_\nu V_e}{\Delta m_{31}^2}, \quad A_n \equiv \frac{2E_\nu V_n}{\Delta m_{31}^2}, \quad \Delta \equiv \frac{\Delta m_{31}^2 L}{4E_\nu}. \quad (2.2)$$

Our analysis is motivated by the observation that θ_{13} and α are small quantities and the active-sterile mixing angles θ_{14} , θ_{24} , and θ_{34} are also expected to be small. Our approach will consist of perturbative expansions in these small quantities. We define an accounting parameter $\lambda \equiv 0.2$ and use

$$\alpha = 0.03 \sim O(\lambda^2), \quad s_{13} \simeq 0.14 \sim O(\lambda), \quad s_{14}, s_{24}, s_{34} \sim O(\lambda), \quad (2.3)$$

where $s_{ij} \equiv \sin(\theta_{ij})$.

In order to calculate the probability, we employ the Cayley-Hamilton theorem [81], which states that any function $g(\mathbb{X})$ of a matrix \mathbb{X} may be expressed as

$$g(\mathbb{X}) = \sum_{i=1}^k X_i g(\Lambda_i), \quad \text{with} \quad X_i \equiv \prod_{j=1, j \neq i}^k \frac{1}{\Lambda_i - \Lambda_j} (\mathbb{X} - \Lambda_j \mathbb{I}). \quad (2.4)$$

Here, Λ_i 's are the distinct eigenvalues of the matrix \mathbb{X} . We identify $\mathbb{X} \equiv -i\mathcal{H}_{3+1}L$ so that the probability amplitude matrix in the flavor basis,

$$\mathcal{A}_f \equiv \exp(-i\mathcal{H}_{3+1}L) = \exp(\mathbb{X}), \quad (2.5)$$

can be calculated. This gives the amplitude for oscillation from ν_α to ν_β as $A(\nu_\alpha \rightarrow \nu_\beta) = [\mathcal{A}_f]_{\beta\alpha}$. The probability is obtained from the amplitude as $P_{\alpha\beta} = |A(\nu_\alpha \rightarrow \nu_\beta)|^2$.

We first calculate the eigenvalues of \mathbb{X} in the presence of sterile neutrinos, with exact dependence on Δm_{41}^2 and matter effect, as a perturbative expansion in the small parameters listed in eq. (2.3). Using the eigenvalues, we calculate the amplitude $A(\nu_\mu \rightarrow \nu_e)$ and the conversion probability $P_{\mu e}$. In the next section, we shall present an explicit expression for the probability calculated up to $O(\lambda^3)$.

2.1 Decoupling of θ_{24} and θ_{34} -dependent terms in matter

The analytic expression for the conversion probability $P_{\mu e}$, correct up to $O(\lambda^3)$, is

$$\begin{aligned}
P_{\mu e} = & 4 s_{13}^2 s_{23}^2 \frac{\sin^2 [(A_e - 1) \Delta]}{(A_e - 1)^2} \\
& + 2 \alpha s_{13} \sin 2\theta_{12} \sin 2\theta_{23} \cos(\delta_{13} + \Delta) \frac{\sin [(A_e - 1) \Delta]}{A_e - 1} \frac{\sin [A_e \Delta]}{A_e} \\
& + 4 s_{13} s_{14} s_{24} s_{23} \frac{\sin [(A_e - 1) \Delta]}{A_e - 1} \\
& \times R \left[A_n s_{23}^2 \frac{\sin [(A_e - 1) \Delta + \delta'_{24}]}{(A_e - 1)(A_n + 1 - R)} + A_n c_{23}^2 \frac{\sin [(A_e + 1) \Delta + \delta'_{24}]}{A_e (A_n - R)} \right. \\
& - \left(R - \frac{A_n s_{23}^2}{A_n + 1 - R} \right) \frac{\sin [(A_e + 2A_n - 2R + 1) \Delta + \delta'_{24}]}{(A_n - R)(A_e + A_n - R)} \\
& \left. - \left(c_{23}^2 \frac{A_n}{A_e} - [A_e + A_n - 1] \right) \frac{\sin [(A_e - 1) \Delta - \delta'_{24}]}{(A_e - 1)(A_e + A_n - R)} \right] \\
& + 4 s_{13} s_{14} s_{34} s_{23}^2 c_{23} A_n \frac{\sin [(A_e - 1) \Delta]}{A_e - 1} \\
& \times R \left[\frac{\sin [\Delta (A_e - 1) + \delta'_{34}]}{(A_e - 1)(A_n + 1 - R)} + \frac{\sin [(A_e + 2A_n - 2R + 1) \Delta + \delta'_{34}]}{(A_n + 1 - R)(A_n - R)(A_e + A_n - R)} \right. \\
& \left. - \frac{\sin [(A_e + 1) \Delta + \delta'_{34}]}{A_e (A_n - R)} + \frac{\sin [(A_e - 1) \Delta - \delta'_{34}]}{A_e (A_e - 1)(A_e + A_n - R)} \right] + O(\lambda^4). \quad (2.6)
\end{aligned}$$

Here, δ'_{24} and δ'_{34} are defined as $\delta'_{24} \equiv \delta_{24} + \delta_{13}$ and $\delta'_{34} \equiv \delta_{34} + \delta_{13}$, since both δ_{24} and δ_{34} appear only in this combination. Note that the above expression includes the exact dependence on $R \equiv \Delta m_{41}^2 / \Delta m_{31}^2$ (i.e. on Δm_{41}^2) as well as on the constant density matter potentials A_e and A_n .

The first two terms in eq. (2.6) are simply the three-neutrino (3ν) contributions to $P_{\mu e}$ [82], whereas the last two terms are the contributions due to sterile neutrinos. Note that the θ_{24} dependence appears only in the third term, and the θ_{34} dependence appears only in the fourth term. Thus, these two contributions are decoupled as long as the assumption of the smallness of the sterile mixing angles is valid. While the θ_{24} contribution is present even in the vacuum limit, the θ_{34} dependent term is non-zero when $A_n \neq 0$, i.e. only in the presence of matter effects. The θ_{34} contribution may be observed to be suppressed by a factor of $s_{23} c_{23} \simeq 0.5$ as compared to the θ_{24} contribution.

We also observe that the sterile neutrino contributions are regulated by

$$\sin [(A_e - 1) \Delta] / (A_e - 1). \quad (2.7)$$

This dependence also appears in the first two terms in eq. (2.6) that represent the contributions from the active neutrino sector. Thus a significant contribution from the sterile oscillation is expected to be present near $|(A_e - 1)\Delta| = \pi/2$, i.e. near the first oscillation peak while approaching from higher energies. Further dependence of the sterile oscillation peaks on Δm_{41}^2 and matter effects will be discussed throughout this paper.

The probability for $P_{\bar{\mu}e} \equiv P(\bar{\nu}_\mu \rightarrow \bar{\nu}_e)$ is obtained by the replacements

$$A_e \rightarrow -A_e, \quad A_n \rightarrow -A_n, \quad \delta_{ij} \rightarrow -\delta_{ij}. \quad (2.8)$$

Note that the analytic expression in eq. (2.6) is a perturbative expansion in α , therefore the expression is only valid for $\alpha\Delta \lesssim 1$, i.e. when the distance travelled by the neutrinos is much less than the wavelengths of oscillation due to Δm_{21}^2 . For long-baseline and atmospheric neutrino experiments, this is a valid approximation.

2.2 $P_{\mu e}$ in the $\sin(x)/x$ form, with $A_n = -A_e/2$

It may be observed that the terms in eq. (2.6) consist of many quantities with the functional form $\sin(x)/x$. This function reaches a maximum in the limit $x \rightarrow 0$. Therefore it is expected that the contribution of such terms will be significant when the corresponding denominator vanishes, without giving rise to any unphysical singularities. Re-structuring the probability expression in eq. (2.6) as a summation of $\sin(x)/x$ terms will allow us to identify the regions where certain contributions will be dominant.

Further, for the Earth's crust, we can take $A_n \approx -A_e/2$. This is a very good approximation, since the neutral current and the charged current potentials are related via

$$A_n = -\frac{A_e N_n}{2 N_e}, \quad (2.9)$$

and the number of neutrons and electrons are approximately equal for lighter elements. The restructured expression is

$$\begin{aligned} P_{\mu e} = & 4 s_{13}^2 s_{23}^2 \frac{\sin^2 [(A_e - 1)\Delta]}{(A_e - 1)^2} \\ & + 2 \alpha s_{13} \sin 2\theta_{12} \sin 2\theta_{23} \cos(\delta_{13} + \Delta) \frac{\sin [(A_e - 1)\Delta]}{A_e - 1} \frac{\sin [A_e \Delta]}{A_e} \\ & + 4 s_{13} s_{14} s_{24} s_{23} \frac{\sin [(A_e - 1)\Delta]}{A_e - 1} \left[\sin(\delta'_{24}) P_{24}^s + \cos(\delta'_{24}) P_{24}^c \right] \\ & + 4 s_{13} s_{14} s_{34} s_{23}^2 c_{23} \frac{\sin [(A_e - 1)\Delta]}{A_e - 1} \left[\sin(\delta'_{34}) P_{34}^s + \cos(\delta'_{34}) P_{34}^c \right] + O(\lambda^4), \quad (2.10) \end{aligned}$$

where the quantities P_{24}^s , P_{24}^c , P_{34}^s , P_{34}^c can be written using expressions of the $\sin(x)/x$ form as follows. The coefficients of $\sin \delta'_{24}$ and $\cos \delta'_{24}$ terms are, respectively,

$$\begin{aligned} P_{24}^s = & R \left[\frac{1}{2} A_e c_{23}^2 + (R - 1) (s_{23}^2 + 1) \right] \frac{\sin \left[\left(R - 1 + \frac{A_e}{2} \right) \Delta \right]}{R - 1 + \frac{A_e}{2}} \frac{\sin \left[\left(R - \frac{A_e}{2} \right) \Delta \right]}{R - \frac{A_e}{2}} \\ & + c_{23}^2 R \sin \left[\left(R - 1 - \frac{A_e}{2} \right) \Delta \right] \frac{\sin \left[\left(R + \frac{A_e}{2} \right) \Delta \right]}{R + \frac{A_e}{2}}, \quad (2.11) \end{aligned}$$

$$\begin{aligned}
P_{24}^c &= \frac{R}{R - \frac{1}{2}} \left(\left[R - \frac{1}{2} s_{23}^2 - \frac{1}{2} \right] \cos \left[\left(R - 1 + \frac{A_e}{2} \right) \Delta \right] \frac{\sin \left[\left(R - \frac{A_e}{2} \right) \Delta \right]}{R - \frac{A_e}{2}} \right. \\
&\quad \left. + s_{23}^2 \frac{\sin \left[\left(A_e - 1 \right) \Delta \right]}{A_e - 1} + s_{23}^2 (R - 1) \cos \left[\left(R - \frac{A_e}{2} \right) \Delta \right] \frac{\sin \left[\left(R - 1 + \frac{A_e}{2} \right) \Delta \right]}{R - 1 + \frac{A_e}{2}} \right) \\
&\quad + c_{23}^2 R \cos \left[\left(R - 1 - \frac{A_e}{2} \right) \Delta \right] \frac{\sin \left[\left(R + \frac{A_e}{2} \right) \Delta \right]}{R + \frac{A_e}{2}} . \tag{2.12}
\end{aligned}$$

Similarly, the coefficients of $\sin \delta'_{34}$ and $\cos \delta'_{34}$ terms are, respectively,

$$\begin{aligned}
P_{34}^s &= R \left(R - 1 - \frac{A_e}{2} \right) \frac{\sin \left[\left(R - 1 + \frac{A_e}{2} \right) \Delta \right]}{R - 1 + \frac{A_e}{2}} \frac{\sin \left[\left(R - \frac{A_e}{2} \right) \Delta \right]}{R - \frac{A_e}{2}} \\
&\quad - R \sin \left[\left(R - 1 - \frac{A_e}{2} \right) \Delta \right] \frac{\sin \left[\left(R + \frac{A_e}{2} \right) \Delta \right]}{R + \frac{A_e}{2}} , \tag{2.13}
\end{aligned}$$

$$\begin{aligned}
P_{34}^c &= \frac{R}{R - \frac{1}{2}} \left(\frac{\sin \left[\left(A_e - 1 \right) \Delta \right]}{A_e - 1} - \frac{1}{2} \cos \left[\left(R - 1 + \frac{A_e}{2} \right) \Delta \right] \frac{\sin \left[\left(R - \frac{A_e}{2} \right) \Delta \right]}{R - \frac{A_e}{2}} \right. \\
&\quad \left. + (R - 1) \cos \left[\left(R - \frac{A_e}{2} \right) \Delta \right] \frac{\sin \left[\left(R - 1 + \frac{A_e}{2} \right) \Delta \right]}{R - 1 + \frac{A_e}{2}} \right) \\
&\quad - R \cos \left[\left(R - 1 - \frac{A_e}{2} \right) \Delta \right] \frac{\sin \left[\left(R + \frac{A_e}{2} \right) \Delta \right]}{R + \frac{A_e}{2}} . \tag{2.14}
\end{aligned}$$

From the above expressions, we immediately observe that for $R = 1 - A_e/2$ and $R = \pm A_e/2$, the sterile neutrino contribution to $P_{\mu e}$ will be enhanced due to resonance in matter.

In the vacuum limit the θ_{34} dependence vanishes, i.e. $P_{34}^s|_{\text{vac}} = 0$ and $P_{34}^c|_{\text{vac}} = 0$. On the other hand, the P_{24}^s and the P_{24}^c terms can be expressed as

$$\begin{aligned}
P_{24}^s|_{\text{vac}} &\simeq 2 \sin \left[\left(R - 1 \right) \Delta \right] \sin \left[R \Delta \right] , \\
P_{24}^c|_{\text{vac}} &\simeq 2 \cos \left[\left(R - 1 \right) \Delta \right] \sin \left[R \Delta \right] . \tag{2.15}
\end{aligned}$$

In vacuum these simple expressions can give the positions of the peaks and dips due to sterile neutrino oscillations. For a given value of R chosen by Nature, matter effects will be significant around $A_e \approx \pm 2R$ and $A_e = 2(1 - R)$ and will modify the values of P_{24}^s , P_{24}^c , P_{34}^s , and P_{34}^c .

The insights from the eqs. (2.11)-(2.14) in this section determine the positions and amplitudes of peaks and dips in $P_{\mu e}$, and can be used to probe the sensitivity of long baseline experiments to sterile neutrino mass ordering.

2.3 Effects of sterile mass ordering on $P_{\mu e}$ at DUNE

The sensitivity of the oscillation probability $P_{\mu e}$ to the mass ordering in the sterile sector may be examined using the quantity

$$\delta P_{\mu e} = P_{\mu e}(R) - P_{\mu e}(-R) . \tag{2.16}$$

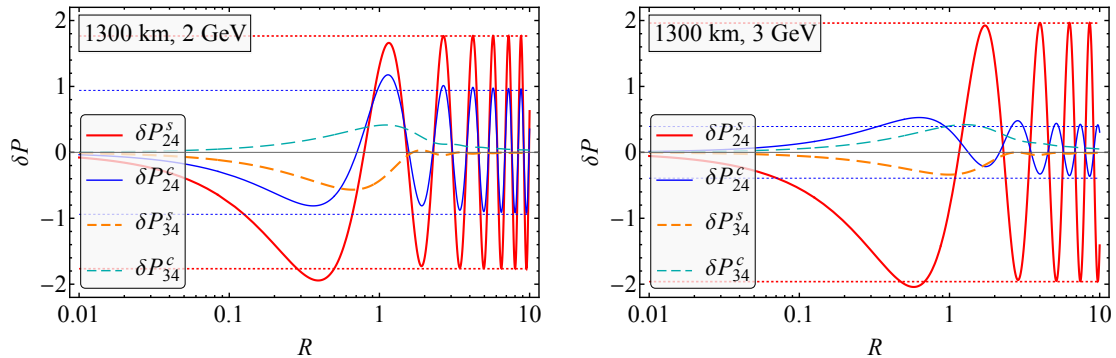


Figure 1. The values of δP_{24}^s , δP_{24}^c , δP_{34}^s and δP_{34}^c as functions of $R = \Delta m_{41}^2 / \Delta m_{31}^2$, at $E_\nu = 2$ GeV [left] and $E_\nu = 3$ GeV [Right], for DUNE. The Horizontal dotted line are the bounds on the amplitude of δP_{24}^s and δP_{24}^c in the vacuum limit, obtained from eq. (2.18).

This quantity clearly depends on δP_{24}^s , δP_{24}^c , δP_{34}^s and δP_{34}^c where ‘ δ ’ indicates the difference between the values of these quantities for positive and negative values of R . Indeed,

$$\begin{aligned} \delta P_{\mu e} = & 4 s_{13} s_{14} s_{24} s_{23} \frac{\sin[(A_e - 1)\Delta]}{A_e - 1} \left[\sin(\delta'_{24}) \delta P_{24}^s + \cos(\delta'_{24}) \delta P_{24}^c \right] \\ & + 4 s_{13} s_{14} s_{34} s_{23}^2 c_{23} \frac{\sin[(A_e - 1)\Delta]}{A_e - 1} \left[\sin(\delta'_{34}) \delta P_{34}^s + \cos(\delta'_{34}) \delta P_{34}^c \right]. \end{aligned} \quad (2.17)$$

To understand the contributions of various δP 's, we plot their values at $E_\nu = 2$ and 3 GeV in figure 1. These energies are in the range where the flux of DUNE is near its maximum and where the first oscillation peak is expected to be observed. It may be seen that all four quantities have significant non-zero values, depending on the value of R .

Note that the quantities δP_{34}^s and δP_{34}^c , which are expected to vanish in the vacuum limit, are non-zero due to the inclusion of matter effects. While δP_{24}^s and δP_{24}^c are non-zero in vacuum:

$$\delta P_{24}^s(\text{vac}) = -2 \sin(2R\Delta) \sin(\Delta), \quad \delta P_{24}^c(\text{vac}) = +2 \sin(2R\Delta) \cos(\Delta), \quad (2.18)$$

their detailed behavior is affected by matter effects. For example, the first oscillation peak would be at $\Delta = \pi/2$ in vacuum, where $\delta P_{24}^c(\text{vac})$ would vanish. However in matter, the first oscillation peak can be approximated to be at $(1 - A_e)\Delta = \pi/2$. Since

$$A_e \approx 2.95 \times 10^{-2} \left(\frac{E_\nu}{1 \text{ GeV}} \right) \left(\frac{\rho}{1 \text{ g/cc}} \right), \quad (2.19)$$

we have $A_e \simeq 0.2$, for $E_\nu \sim 2.5$ GeV at DUNE. As a result, both δP_{24}^s and δP_{24}^c will be non-zero at the first oscillation peak. From eq. (2.17), this implies that DUNE would be sensitive¹ to sterile mass ordering for all possible values of δ'_{24} .

Note that the effects of matter-induced resonance at $A_e = 2(1 - R)$ and $A_e = \pm 2R$ cannot be accounted for by the simple vacuum limit approximations given above in eq. (2.18). The effects of these resonances will be discussed in detail in section 3.

¹Note that for T2K and NOVA, due to smaller matter effects, δP_{24}^c would be small at all oscillation peaks. This leads to a strong dependence of the sterile mass ordering sensitivity to the value of δ'_{24} .

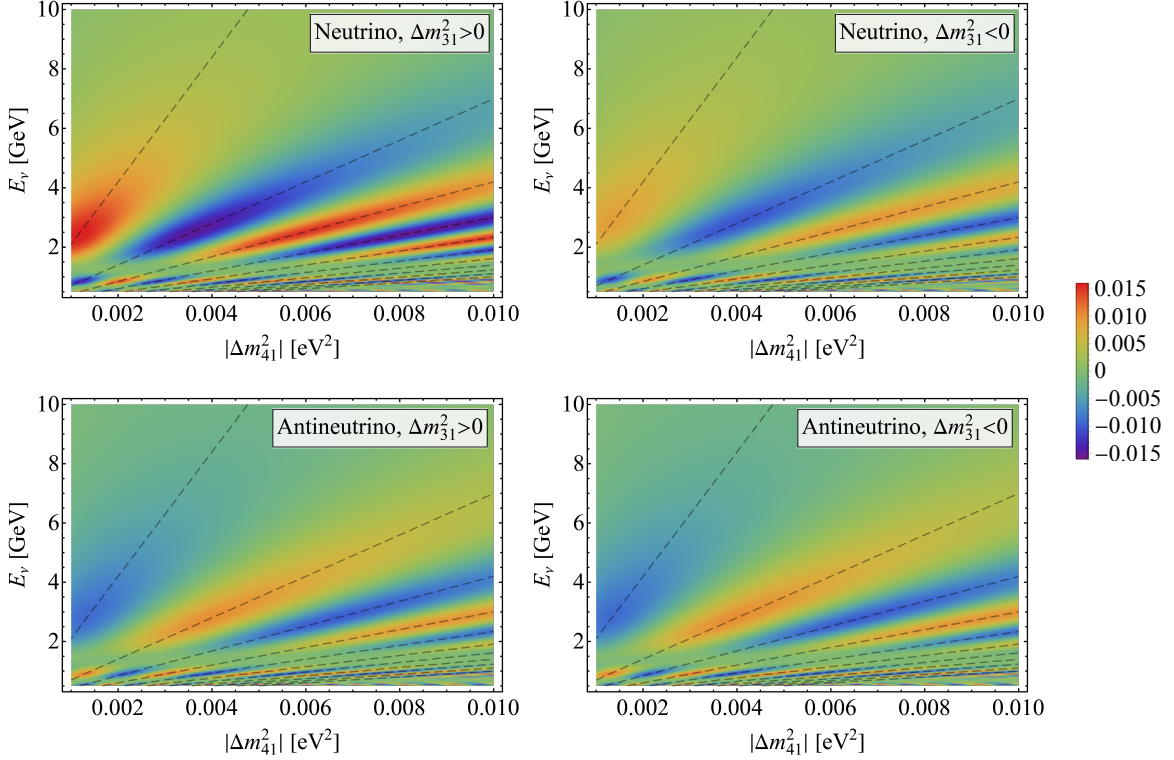


Figure 2. $\delta P_{\mu e}$ [Top panels] and $\delta P_{\bar{\mu} \bar{e}}$ [Bottom panels] in the $(\Delta m_{41}^2 - E_\nu)$ plane at $L = 1300$ km for the mixing parameters given in eqs. (2.20)-(2.21). Left and Right panels correspond to Normal and Inverted mass ordering, respectively, in the active sector.

For our analysis, we choose the benchmark parameters in the 3ν sector to be

$$\begin{aligned}
 |\Delta m_{31}^2| &= 2.5 \times 10^{-3} \text{ eV}^2, & \Delta m_{21}^2 &= 7.5 \times 10^{-5} \text{ eV}^2, & \delta_{13} &= -90^\circ, \\
 \theta_{12} &= 33.56^\circ, & \theta_{23} &= 45^\circ, & \theta_{13} &= 8.46^\circ.
 \end{aligned}
 \tag{2.20}$$

This is consistent with the global fits [3, 4]. We choose the sterile sector parameter values as

$$\theta_{14} = 5^\circ, \quad \theta_{24} = 10^\circ, \quad \theta_{34} = 0^\circ, \quad \delta_{24} = 0^\circ, \quad \delta_{34} = 0^\circ.
 \tag{2.21}$$

With the above choice, only the P_{24}^s contribution due to sterile neutrinos will stay. This simplifies the analytic exploration of the features of $P_{\mu e}$. Later in section 3, we shall find that many features in sensitivity to sterile mass ordering as a function of $|\Delta m_{41}^2|$ can be explained by observing the behavior of P_{24}^s in matter.

We plot $\delta P_{\mu e}$ and $\delta P_{\bar{\mu} \bar{e}}$ in the $(\Delta m_{41}^2, E_\nu)$ plane in figure 2, and observe that the sensitivity to sterile mass ordering depends on whether we are observing neutrinos or anti-neutrinos, as well as on the sign of Δm_{31}^2 (normal or inverted mass ordering of active neutrinos). The following observations may be made from figure 2

- The values of $|\delta P_{\mu e}|$ and $|\delta P_{\bar{\mu} \bar{e}}|$ are observed to be maximum at $E_\nu \sim 2 - 3$ GeV. This is primarily due to the $\sin[(1 - A_e)\Delta]/(1 - A_e)$ dependence of the sterile contribution, as obtained in eq. (2.17).

- The peaks and valleys of $\delta P_{\mu e}$ and $\delta P_{\bar{\mu} e}$ correspond approximately to the $\sin(2R\Delta)$ dependence of the δP_{24}^s term in eq. (2.18). This dependence is represented by the black dashed lines in figure 2.
- For higher values of Δm_{41}^2 (i.e. $R \gg 1$), we observe the expected rapid oscillation at low energies.
- The amplitudes of the peaks and dips are maximum for neutrino with $\Delta m_{31}^2 > 0$.
- The locations of peaks and valleys approximately interchange between ν and $\bar{\nu}$ plots. This is because the only non-zero contribution to $|\delta P_{\mu e}|$ is from δP_{24}^s , which is the coefficient of $\sin(\delta'_{24})$, and $\delta_{ij} \rightarrow -\delta_{ij}$ when $\nu \rightarrow \bar{\nu}$.

When a non-zero contribution of P_{24}^c is present, we expect the dependence of $\delta P_{\mu e}$ on Δm_{41}^2 and E_ν to change, however eqs. (2.11)-(2.14) can explain the dominant characteristics of $\delta P_{\mu e}$ in such a scenario.

2.4 Peaks and dips in $P_{\mu e}$ at DUNE due to sterile neutrino

The analytic expressions in Eqs. (2.10)-(2.14) can explain the features of sterile neutrino contributions to $P_{\mu e}$ quite well, as can be seen in figure 3. We choose $|\Delta m_{41}^2| = 8 \times 10^{-3} \text{ eV}^2$ ($R = 3.2$) for comparison between the numerical and analytic solutions. Plotting $P(\nu_\mu \rightarrow \nu_e)$ and $P(\bar{\nu}_\mu \rightarrow \bar{\nu}_e)$ for normal and inverted mass ordering (in both the sectors) in figure 3, we observe that the two sterile mass orderings lead to distinctly different shapes of the conversion probability. For both the neutrino and antineutrino channels, with normal or inverted mass ordering (in the active or the sterile sector), our analytic approximations follow the exact numerical results with an absolute accuracy of better than $\sim 1\%$. Typically the sterile contribution results in additional peaks and dips which are more visible near the first oscillation peak of the 3ν sector. The positions and the amplitudes of the sterile as well as the 3ν peaks and dips are observed to be reproduced extremely well.

The positions and amplitudes of these peaks and dips may be understood by separating the dominant frequencies in P_{24}^s :

$$P_{24}^s \equiv C_-^s \cos[(1 - A_e)\Delta] + C_+^s \cos[(1 + A_e)\Delta] + C_R^s \cos[(1 - 2R)\Delta]. \quad (2.22)$$

Here, the coefficients C_-^s , C_+^s and C_R^s are smoothly varying (non-oscillating) functions of R , A_e and θ_{23} , that regulate the amplitudes of peaks and dips, but do not affect their positions. Examining each of the terms in eq. (2.22), we can account for the oscillatory behaviors of the sterile neutrino contributions:

- The first term in eq. (2.22) oscillates as $\cos[(1 - A_e)\Delta]$. This term will contribute maximally at $(1 - A_e)\Delta = n\pi$ i.e. at the dips of the 3ν contribution. This term will therefore modify the probability near the dips of $P_{\mu e}$, and hence will affect the determination of θ_{23} if sterile neutrinos are present.
- The second term in eq. (2.22), which oscillates as $\cos[(1 + A_e)\Delta]$, is not present in the 3ν sector. However, note that the numerical value of this frequency for the ν channel is half of the leading order 3ν frequency for the $\bar{\nu}$ channel, and vice versa ($\nu \leftrightarrow \bar{\nu}$).

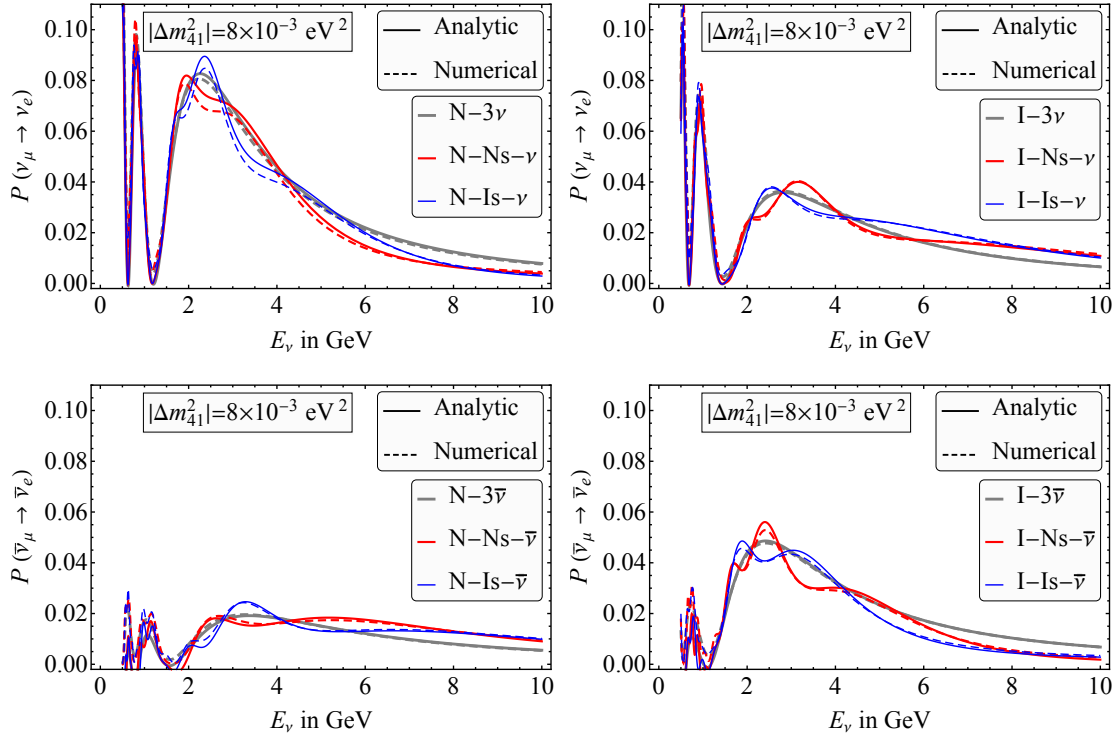


Figure 3. Conversion probabilities $P(\nu_\mu \rightarrow \nu_e)$ [Top panels] and $P(\bar{\nu}_\mu \rightarrow \bar{\nu}_e)$ [Bottom panels] as functions of energy (E_ν) for $L = 1300$ km, for the mixing parameters given in eqs. (2.20)-(2.21) and for $|\Delta m_{41}^2| = 8 \times 10^{-3} \text{ eV}^2$. Left and Right panels correspond to Normal and Inverted mass ordering, respectively, in the active sector.

- Exploring the final term of eq. (2.22), we expect the sterile-induced peaks and dips to be at the extrema of $\cos[(1 - 2R)\Delta]$. Note that this frequency has no matter dependence. For $R > 1$, this is the term which would induce oscillations at an energy higher than in the 3 ν case. The sign of this contribution would depend on the sign of $C_R^s \sin(\delta'_{24})$. We can write

$$C_R^s = -\frac{1}{2}R \left(\frac{1}{A_e + 2R} + \frac{A_e + 6R - 6}{(2R - A_e)(A_e + 2R - 2)} \right). \quad (2.23)$$

For $E_\nu = 0.5 - 10$ GeV, with our parameter choices both C_R^s and $\sin(\delta'_{24})$ are negative. Therefore, the net sterile contribution peaks at $\cos[(1 - 2R)\Delta] = 1$ and dips at $\cos[(1 - 2R)\Delta] = -1$, as can be seen in figure 3. Indeed, we can even calculate the positions of peaks and dips induced by sterile neutrinos. For example, the first two peaks and dips in the N-Ns- ν scenario (Top left in figure 3) can be seen to be at $(1 - 2R)\Delta = 2\pi, 4\pi$ and $(1 - 2R)\Delta = \pi, 3\pi$ respectively:

$$E_\nu^{\text{peak}} \simeq 3.55 \text{ GeV}, 1.77 \text{ GeV}, \quad E_\nu^{\text{dip}} \simeq 7.1 \text{ GeV}, 2.37 \text{ GeV}. \quad (2.24)$$

Note that, though the peak and dip position are independent of matter effects, their amplitudes can have substantial matter dependence, as can be seen from eq. (2.23).

While the above discussion has been for N-Ns mass ordering in the neutrino sector, a similar analytic understanding for sterile peaks and dips may also be obtained for all the remaining mass ordering scenarios, viz. N-Is, I-Ns and I-Is, and also for antineutrinos.

In the next section, we will explore the sensitivity of DUNE to sterile mass ordering. The dependence of the sensitivity on Δm_{41}^2 can be explained using our analytic expressions obtained in this section.

3 Sensitivity to sterile mass ordering at DUNE

DUNE (Deep Underground Neutrino Experiment) is an upcoming long-baseline experiment in the USA. It will consist of a neutrino source facility located at Fermilab and a far detector located at the Sanford Underground Research Facility in South Dakota, and thus will have a baseline of 1300 km. The primary aim of DUNE is to probe all the three unknowns in the 3ν oscillation sector, viz., the leptonic CP violation, the neutrino mass ordering and the octant of θ_{23} . The accelerator at Fermilab will generate a proton beam of energy 80–120 GeV at 1.2–2.4 MW which will finally produce a neutrino beam of a wide energy range 0.5–8.0 GeV. The far detector will consist of four identical 10 kt LArTPC (Liquid Argon Time Projection Chamber) detectors with a total fiducial mass of 40 kt. We have used the General Long Baseline Experiment Simulator (GLOBES) package [83, 84] to simulate the DUNE data. The detector-related specifications used in this study are listed in table 2. The neutrino oscillation parameter values used here are given in table 3.

Detector details	Normalization error		Energy calibration error	
	Signal	Background	Signal	Background
Baseline = 1300 km Runtime (yr) = 3.5 ν + 3.5 $\bar{\nu}$ 40 kton, LArTPC $\varepsilon_{app} = 80\%$, $\varepsilon_{dis} = 85\%$ $R_e = 0.15/\sqrt{E_\nu(\text{GeV})}$, $R_\mu = 0.20/\sqrt{E_\nu(\text{GeV})}$	$\nu_e : 5\%$	$\nu_e : 10\%$	$\nu_e : 5\%$	$\nu_e : 5\%$
	$\nu_\mu : 5\%$	$\nu_\mu : 10\%$	$\nu_\mu : 5\%$	$\nu_\mu : 5\%$

Table 2. Details of detector configurations, efficiencies, resolutions, and systematic uncertainties for DUNE. Here, ε_{app} and ε_{dis} are signal efficiencies for ν_e^{CC} and ν_μ^{CC} respectively. Also, R_e and R_μ are energy resolutions for ν_e^{CC} and ν_μ^{CC} events respectively. One year of runtime corresponds to 1.47×10^{21} POT (protons on target).

3.1 Analysis procedure

We simulate the data by using the input (“true”) values of the parameters as given in table 3, and try to fit the data with alternative (“test”) values of these parameters, corresponding to the opposite sterile mass ordering. The quantity $\Delta\chi_{\text{SMO}}^2$ that quantifies the sensitivity of DUNE to sterile mass ordering is defined as

$$\Delta\chi_{\text{SMO}}^2 \equiv \chi^2(\text{test}) - \chi^2(\text{true}) , \quad (3.1)$$

Sector	Parameter	Value	Variation range
Active	θ_{12}	33.56°	–
	θ_{13}	8.46°	–
	θ_{23}	45°	$[40^\circ, 50^\circ]$
	δ_{13}	-90°	$[-180^\circ, 0^\circ]$
	Δm_{21}^2	$7.5 \times 10^{-5} \text{ eV}^2$	–
	Δm_{31}^2	$2.5 \times 10^{-3} \text{ eV}^2$	–
Sterile	θ_{14}	5°	$[0^\circ - \theta_{14}^{\max}]$
	θ_{24}	10°	$[0^\circ - 55^\circ]$
	θ_{34}	0	–
	δ_{24}	0	$[-180^\circ, 180^\circ]$
	δ_{34}	0	–
	Δm_{41}^2	$\Delta m_{41}^2(\text{true})$	$\Delta m_{41}^2(\text{true}) \pm 15\%$

Table 3. The simulated (true) values of parameters in the active and sterile sectors, and the variation ranges taken for their test values.

where the value of χ^2 is obtained using the GLOBES package [83, 84]. We further perform minimization of $\chi^2(\text{test})$ by varying over the fitting parameters to take care of the effects of their uncertainties. The range of variation of the neutrino oscillation parameters has been given in table 3.

Among the active neutrino mixing parameters, θ_{12} and Δm_{21}^2 are not expected to affect the identification of sterile mass ordering. Further, the values of θ_{13} and Δm_{31}^2 are known to high precision, so we do not vary over these four parameters. We also take the mass ordering in the active neutrino sector to be known. However, we vary over θ_{23} and δ_{13} , which have large uncertainties.

In the sterile sector, we choose to restrict our analysis to $\theta_{34}(\text{test}) = 0$, i.e. we do not vary over θ_{34} for the sake of practicality. This also makes the value of δ_{34} irrelevant, allowing us to focus on the dominant effects of P_{24}^s . We then vary over the two mixing angles θ_{14} and θ_{24} , the CP violating phase δ_{24} , and the mass squared difference Δm_{41}^2 , in the ranges shown in table 3. For the range of θ_{24} , we use a conservative upper bound based on constraints from MINOS and MINOS+ [85, 86]. For θ_{14} , we use a conservative upper bound based on the constraints from Daya Bay/Bugey-3 [85] as well as those from $\sin^2 \theta_{\mu e} \equiv \sin^2 2\theta_{14} \sin^2 \theta_{24}$ at MINOS and MINOS+ [86]. Our variation range for Δm_{41}^2 considers a $\pm 15\%$ error in its measurement ².

²If DUNE observes sterile neutrinos with $|\Delta m_{41}^2| \lesssim O(10^{-2}) \text{ eV}^2$, then it would measure the active-sterile oscillation phase with a precision of

$$\frac{\delta\phi}{2\pi} = \frac{1}{2\pi} \frac{\Delta m_{41}^2 L}{4E_\nu} \frac{\delta E_\nu}{E_\nu} < 0.14 \quad (3.2)$$

for $E_\nu > 2 \text{ GeV}$, where we have taken the energy resolution $\delta E_\nu/E_\nu = 0.15/\sqrt{E_\nu(\text{GeV})}$. This is the same as the precision in Δm_{41}^2 . Therefore, we can safely take the precision in Δm_{41}^2 to be better than $\pm 15\%$ in this low- Δm_{41}^2 range. As we will see later in this section, the sensitivity to sterile mass ordering is very low for $\Delta m_{41}^2 \gtrsim 10^{-2} \text{ eV}^2$. Hence, the precision in this high- Δm_{41}^2 range will not matter in our analysis.

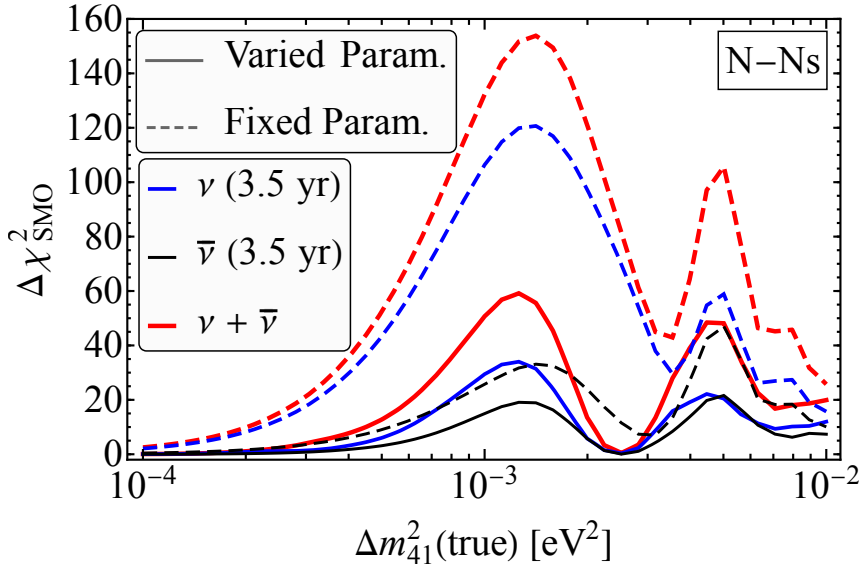


Figure 4. Dependence of $\Delta\chi_{\text{SMO}}^2$ on Δm_{41}^2 , for the N-Ns ($\Delta m_{31}^2 > 0, \Delta m_{41}^2 > 0$) scenario. The dashed curves are obtained by using fixed test values of neutrino mixing parameters. The solid curves are obtained by varying the test values in the ranges indicated in table 3. The neutrino and the antineutrino runs are taken to be for 3.5 years each.

3.2 Dependence of the sensitivity on $|\Delta m_{41}^2|$

The sensitivity to sterile mass ordering at DUNE calculated over a wide range of $|\Delta m_{41}^2|$ is shown in figure 4, taking the N-Ns scenario ($\Delta m_{31}^2 > 0, \Delta m_{41}^2 > 0$). We show the results separately for the 3.5 yr neutrino run, for the 3.5 yr antineutrino run, and their combination. The results are presented for the cases when the test parameters are fixed, as well as when they are varied over their ranges specified in table 3.

The following observations can be made from figure 4:

- In principle, DUNE has sensitivity to sterile mass ordering over the $|\Delta m_{41}^2|$ range of $(10^{-4} - 10^{-2}) \text{ eV}^2$. This is not surprising since one of the major aims of DUNE is to observe the mass ordering around $\Delta m_{31}^2 \approx 2.5 \times 10^{-3} \text{ eV}^2$. For $|\Delta m_{41}^2| < 10^{-4} \text{ eV}^2$, oscillations due to sterile neutrino would not develop for DUNE. For $|\Delta m_{41}^2| > 10^{-2} \text{ eV}^2$, we expect a reduced sensitivity to sterile mass ordering due to multiple reasons, viz. the averaging out of sterile neutrino oscillations, the reduced effect on matter potential terms, and a reduced interference between the frequencies Δm_{31}^2 and Δm_{41}^2 .
- The variation over the uncertainties of the neutrino mixing parameters decreases the sensitivity considerably — almost by a factor of 3. In spite of this, it is observed that over a wide range of $|\Delta m_{41}^2|$ values, it is possible to have $\Delta\chi_{\text{SMO}}^2 \gtrsim 25$ (i.e. a 5σ identification of sterile mass ordering), when neutrino and antineutrino data are combined.

Active ν mass ordering	Sterile ν mass ordering	$\nu/\bar{\nu}$	sign of A_e	sign of R
N	Ns	ν	+	+
		$\bar{\nu}$	-	+
	Is	ν	+	-
		$\bar{\nu}$	-	-
I	Ns	ν	-	-
		$\bar{\nu}$	+	-
	Is	ν	-	+
		$\bar{\nu}$	+	+

Table 4. The signs of A_e and R for all mass ordering combinations, for neutrinos and antineutrinos.

- We observe a dip in sensitivity to sterile mass ordering at $|\Delta m_{41}^2| \approx |\Delta m_{31}^2|$, this is due to possible degeneracy between the sterile and the atmospheric mass squared difference, which makes it difficult to disentangle their contributions.
- The $\Delta\chi_{\text{SMO}}^2$ value in the neutrino (for fixed parameters as well as when they are varied) channel is considerably larger than that in the antineutrino channel. This is expected, since the cross sections for antineutrinos at $\sim\text{GeV}$ energies are approximately half of the neutrino cross sections. However, note that for $\Delta m_{41}^2 > \Delta m_{31}^2$, the sensitivity for the antineutrino channel increases significantly and becomes almost comparable to the neutrino channel sensitivity. The reason for this can be understood by inspecting the P_{24}^s term in eq. (2.11) term that regulates the sterile contribution to $P_{\mu e}$. In the antineutrino channel for the N-Ns scenario, we have a possible resonant behavior at $R > 1$, i.e. for $\Delta m_{41}^2 > \Delta m_{31}^2$, leading to an enhanced change in the conversion probability. However, in the neutrino channel, no such resonances involving sterile neutrinos are possible for the N-Ns scenario and $R > 1$.

The first two observations above will be seen to hold when we later discuss the other three mass ordering combinations, viz. N-Is, I-Ns, and I-Is. The last two observations will be modified depending on the mass ordering combinations. This will be analyzed in the next section.

3.3 Dependence of sensitivity on mass ordering combinations

In the last section, we explored the details of sensitivity to $|\Delta m_{41}^2|$ for the N-Ns scenario. In this section, we will explore this dependence for other scenarios, viz. N-Is, I-Ns, and I-Is, and draw comparisons among them. These differences will be explained by our analytic approximations obtained in section 2. In figure 5, we show the sensitivity to sterile mass ordering for all the above mentioned combinations, for the 3.5 yr neutrino run, 3.5 yr antineutrino run, and their combined statistics. Note that now we only show the results where the neutrino oscillation parameters are varied over their uncertainties.

Before we further discuss the effects of matter potential in the sterile contribution to $P_{\mu e}$, we first document the signs of A_e and R for all possible mass ordering combinations, for both neutrinos and antineutrinos, in table 4. We see that the 8 different

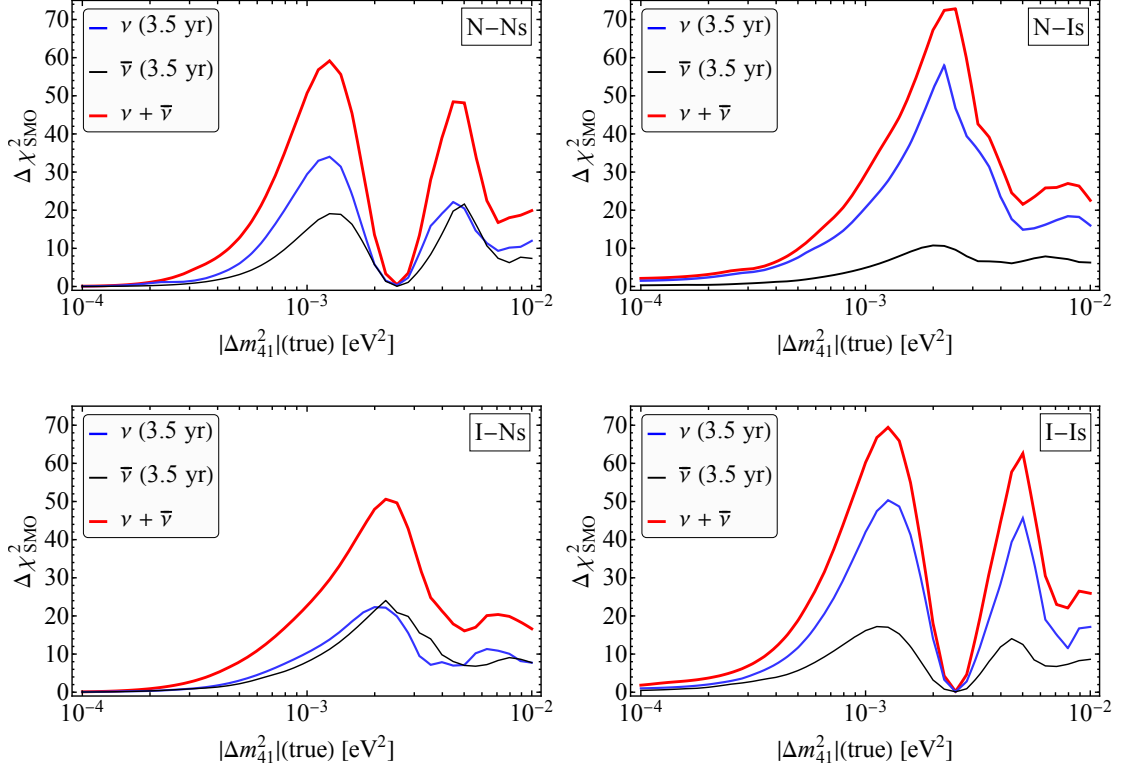


Figure 5. Same as the figure 4, but for all four mass ordering combinations (N-Ns, N-Is, I-Ns, I-Is). We show only the results with test parameters varied over the range indicated in Table 3.

scenarios can be classified into 4 distinct sets corresponding to the sign of A_e and R , viz. $(+, +)$, $(-, +)$, $(+, -)$, $(-, -)$. We expect that the behavior due to matter effect and sterile term will be uniform within these four independent sets. In Fig. 5 we observe that:

- Even taking into account the dilution in sensitivity due to variation over most of the test parameters, DUNE remains sensitive to sterile mass ordering for all mass ordering combinations, for $|\Delta m_{41}^2| \in (10^{-4}, 10^{-2})$ eV².
- For N-Ns and I-Is scenarios, we observe a dip in sensitivity at $|\Delta m_{41}^2| \approx |\Delta m_{31}^2|$. As noted in section 3.2, this is due to the degeneracy between Δm_{31}^2 and Δm_{41}^2 . This degeneracy does not occur in the scenarios N-Is and I-Ns, since the mass squared differences have opposite signs. As a result, the sharp dips present in the earlier two scenarios are absent in these two.
- We observe higher sensitivity in the neutrino channel for N-Ns- ν , N-Is- ν and in the antineutrino channel, for I-Ns- $\bar{\nu}$, I-Is- $\bar{\nu}$. This is due to the enhancement from the $\sin[(A_e - 1)\Delta]/(A_e - 1)$ factor in the sterile contribution to $P_{\mu e}$. One can see from table 4 that for the above mentioned combinations A_e is positive, leading to the enhancement. This is thus due to the interplay between active neutrino mass ordering and matter effects.

sign of A_e	sign of R	Combinations		$ R < 1$	$ R > 1$
		ν	$\bar{\nu}$		
+	+	N-Ns- ν	I-Is- $\bar{\nu}$	✓	—
—	+	I-Is- ν	N-Ns- $\bar{\nu}$	✓	✓✓
+	—	N-Is- ν	I-Ns- $\bar{\nu}$	✓✓	—
—	—	I-Ns- ν	N-Is- $\bar{\nu}$	—	—

Table 5. Modifications in the probabilities $P(\nu_\mu \rightarrow \nu_e)$ and $P(\bar{\nu}_\mu \rightarrow \bar{\nu}_e)$ due to the interplay between Δm_{41}^2 and matter effect. Here dash (‘—’) denotes the absence of significant enhancement due to matter effects. The single tick (‘✓’) denotes a small enhancement and double ticks (‘✓✓’) denote a large enhancement due to possible resonance-like behaviors.

- Similarly, we observe increased sensitivity for N-Is- ν , I-Is- ν in the neutrino channel and for N-Ns- $\bar{\nu}$, I-Ns- $\bar{\nu}$ in the antineutrino channel. This may be explained by the interplay between the two new parameters in the Hamiltonian, $A_n (= -A_e/2)$ and R , that become relevant for sterile neutrino propagation in matter. The resulting $\sin[(R + A_e/2)\Delta]/(R + A_e/2)$ factor in the sterile contribution to P_{24}^s , as shown in eq. (2.11) leads to an enhancement in the (+, −) and (−, +) scenarios in table 4.

In the next section, we shall explore in more detail the possible enhancement in the sensitivity to sterile mass ordering due to the sterile contribution to $P_{\mu e}$ giving rise to resonance-like behaviors, that appear in certain mass ordering combinations in matter.

3.4 Interplay between Δm_{41}^2 and matter effects

For the parameter choices in table 3, the relevant sterile contribution in the conversion channel may be expressed as

$$P_{\mu e}(\text{sterile}) = 4 s_{13} s_{14} s_{24} s_{23} \frac{\sin[(A_e - 1)\Delta]}{A_e - 1} \sin(\delta'_{24}) P_{24}^s. \quad (3.3)$$

Here, the P_{24}^s term [eq. (2.11)] is

$$P_{24}^s = R \left[\frac{1}{2} A_e c_{23}^2 + (R - 1)(s_{23}^2 + 1) \right] \frac{\sin[(R - 1 + \frac{A_e}{2})\Delta]}{R - 1 + \frac{A_e}{2}} \frac{\sin[(R - \frac{A_e}{2})\Delta]}{R - \frac{A_e}{2}} + c_{23}^2 R \sin[(R - 1 - \frac{A_e}{2})\Delta] \frac{\sin[(R + \frac{A_e}{2})\Delta]}{R + \frac{A_e}{2}}. \quad (3.4)$$

The normalized effective matter potential is $A_e \approx 0.09 \times (E_\nu \text{ in GeV})$ for DUNE. Eq. (3.4) indicates that resonance-like behaviors would appear when $A_e \approx 2(1 - R)$ or $A_e \approx \pm 2R$. Resonance due to the first condition would appear only for one of the possible signs of R . Even though the second condition may be satisfied for both signs of R , their coefficients in eq. (3.4) are different. This leads to a different value of P_{24}^s for different signs of ‘ R ’. Therefore, such resonance like behavior may be expected to lead to a higher sensitivity to the sterile mass ordering.

The occurrence and strength of the enhancement in sensitivity due to such resonance-like behaviors is predicted in table 5. We can now explain the following features of figure 5:

- The cross section of neutrinos of GeV energy is higher than those of antineutrinos by a factor of about two. Therefore, in the absence of matter effects, one would expect the sensitivity in the neutrino channel to be about twice that in the antineutrino channel. Major deviations from this naive expectation occur in the following scenarios:
 1. The relative sensitivity in the antineutrino channel is enhanced in the scenarios (i) N-Ns with $|R| > 1$ and (ii) I-Ns with $|R| < 1$. In the first scenario, there is enhancement in the antineutrino channel near $A_e = 2(1 - R)$, which is absent in the neutrino channel. Similarly, in the second scenario, the enhancement is present only in the antineutrino channel near $A_e = -2R$.
 2. The relative sensitivity in the neutrino channel is enhanced in the scenarios (i) I-Is with $|R| > 1$ and (ii) N-Is with $|R| < 1$. In the first scenario, there is enhancement in the neutrino channel near $A_e = 2(1 - R)$, which is absent in the antineutrino channel. Similarly, in the second scenario, the enhancement is present only in the neutrino channel near $A_e = -2R$.
- In the $|R| > 1$ regime, the sensitivity for the N-Ns and I-Is combinations is larger than that for the N-Is and I-Ns mass orderings. This is due to the enhancement in sensitivity for the N-Ns- $\bar{\nu}$ and I-Is- ν probabilities, respectively. Both these combinations belong to the $(-, +)$ set in table 5. For this set, enhancement is expected due to the resonance-like condition near $A_e = 2(1 - R)$. Even among these two mass orderings, the sensitivity for I-Is is more since the enhancement is in the neutrino channel. Such an enhancement does not occur for N-Is and I-Ns mass orderings in ν or $\bar{\nu}$ channels.
- In the $|R| < 1$ regime, the sensitivity in the N-Is mass ordering is high due to a resonance-like behavior near $A_e = -2R$ in the neutrino channel. A similar enhancement occurs for the I-Ns mass ordering, albeit in the antineutrino channel, so the overall enhancement is not as pronounced. Further, for both N-Ns and I-Is mass ordering scenarios, enhancements due to resonance-like behavior can occur in both the ν and $\bar{\nu}$ channels as pointed out in table 5.
- For the I-Ns mass ordering, the sensitivity in the neutrino channel is small, leading to an overall low sensitivity. This is due to the lack of any enhancement in the neutrino channel for this mass ordering.

This demonstrates the power of our analytic approximation for the conversion probability, and the utility of representing it in the $\sin(x)/x$ form as shown in section 2.

4 Conclusions

In this paper, we analytically calculate the conversion probability $P_{\mu e}$ in the presence of sterile neutrinos, with exact dependence on Δm_{41}^2 and with explicit dependence on matter potential. The probability is expressed as a perturbative expansion in the small parameters α , s_{13} , s_{14} , s_{24} and s_{34} . We show that the terms involving s_{24} and s_{34} can be

explicitly separated, with the latter term contributing only in the presence of matter, due to the neutral-current forward-scattering of active neutrinos. Further, we rearrange the probability expression in terms of the $\sin(x)/x$ form and show that the dependence on CP-violating angles in the sterile sector (δ_{24} and δ_{34}) can be separated. This form encapsulates the resonance-like behaviors occurring when matter potentials and Δm_{41}^2 satisfy specific relationships.

To bring out the power of our formalism, we first show that our analytic expression can accurately predict the positions and amplitudes of sterile induced oscillations at a long-baseline experiment like DUNE. We further focus on the identification of sterile mass ordering, i.e. the sign of Δm_{41}^2 , at DUNE, and motivate that such an identification is possible for $\Delta m_{41}^2 \in (10^{-4} - 10^{-2}) \text{ eV}^2$ for a wide choice of neutrino-mixing parameter values. Note that this mass-squared range overlaps the parameter space which can address the tension between T2K and NOvA data. Since the mass-squared scales Δm_{31}^2 and Δm_{41}^2 are comparable to each other in this range, it is important to calculate the explicit contributions of sterile oscillations in matter. Our analytic expressions, therefore, are particularly crucial for probing the effects of sterile neutrinos for such scenarios.

We numerically calculate the sensitivity of DUNE to sterile mass ordering for all the mass ordering combinations in the active and sterile sector. We find that this sensitivity can indeed be significant in the range $\Delta m_{41}^2 \sim (10^{-4} - 10^{-2}) \text{ eV}^2$. This is expected, since DUNE is designed to probe the parameter range around such values. This sensitivity is observed to have intricate dependence on the actual value of Δm_{41}^2 , which, however can be clearly understood by the analytic approximations calculated in this paper. In particular, these approximations can explain the relative sensitivities in neutrino and the antineutrino channel, in the various mass ordering scenarios, in terms of the resonance-like behaviors. The non-trivial effects of the complex interplay between Δm_{41}^2 and the matter effects can thus be clearly understood.

Although our analysis has been focused on DUNE and the identification of sterile mass ordering therein, the expressions for $P_{\mu e}$ that we have calculated would be valid for all current and upcoming long-baseline experiments. In general, they would be valid as long as the matter densities neutrinos propagate through may be approximated by a single line-averaged density. Thus, even for atmospheric neutrinos that do not pass through the core, our expressions would serve as a good approximation which is valid over a wide range of Δm_{41}^2 .

Acknowledgments

The authors would like to acknowledge WHEPP-XVI for their hospitality and arrangements, where initial discussions and work took place. D.S.C. and A.D. acknowledge support from the Department of Atomic Energy (DAE), Government of India, under Project Identification No. RTI4002. D.P. is thankful for the support of FAPESP funding Grant 2014/19164-6 and 2020/04261-7. M.M.D. would like to acknowledge the support of the DST SERB grant EMR/2017/001436. D.S.C. thanks K. Ghadiali for his help regarding the numerical packages.

References

- [1] M. Sajjad Athar et al., *Status and perspectives of neutrino physics*, *Prog. Part. Nucl. Phys.* **124** (2022) 103947 [[arXiv:2111.07586](#)].
- [2] PARTICLE DATA GROUP collaboration, *Review of Particle Physics*, *PTEP* **2022** (2022) 083C01.
- [3] I. Esteban, M.C. Gonzalez-Garcia, M. Maltoni, T. Schwetz and A. Zhou, *The fate of hints: updated global analysis of three-flavor neutrino oscillations*, *JHEP* **09** (2020) 178 [[arXiv:2007.14792](#)].
- [4] NuFIT v5.1 (2021), <http://www.nu-fit.org>.
- [5] P.F. de Salas, D.V. Forero, S. Gariazzo, P. Martínez-Miravé, O. Mena, C.A. Ternes et al., *2020 global reassessment of the neutrino oscillation picture*, *JHEP* **02** (2021) 071 [[arXiv:2006.11237](#)].
- [6] F. Capozzi, E. Di Valentino, E. Lisi, A. Marrone, A. Melchiorri and A. Palazzo, *Unfinished fabric of the three neutrino paradigm*, *Phys. Rev. D* **104** (2021) 083031 [[arXiv:2107.00532](#)].
- [7] HYPER-KAMIOKANDE PROTO- collaboration, *Physics potential of a long-baseline neutrino oscillation experiment using a J-PARC neutrino beam and Hyper-Kamiokande*, *PTEP* **2015** (2015) 053C02 [[arXiv:1502.05199](#)].
- [8] ICAL collaboration, *Physics Potential of the ICAL detector at the India-based Neutrino Observatory (INO)*, *Pramana* **88** (2017) 79 [[arXiv:1505.07380](#)].
- [9] JUNO collaboration, *Neutrino Physics with JUNO*, *J. Phys. G* **43** (2016) 030401 [[arXiv:1507.05613](#)].
- [10] DUNE collaboration, *Deep Underground Neutrino Experiment (DUNE), Far Detector Technical Design Report, Volume II: DUNE Physics*, [arXiv:2002.03005](#).
- [11] DUNE collaboration, *Long-baseline neutrino oscillation physics potential of the DUNE experiment*, *Eur. Phys. J. C* **80** (2020) 978 [[arXiv:2006.16043](#)].
- [12] ALEPH, DELPHI, L3, OPAL, SLD, LEP ELECTROWEAK WORKING GROUP, SLD ELECTROWEAK GROUP, SLD HEAVY FLAVOUR GROUP collaboration, *Precision electroweak measurements on the Z resonance*, *Phys. Rept.* **427** (2006) 257 [[hep-ex/0509008](#)].
- [13] R.N. Mohapatra and P.B. Pal, *Massive Neutrinos in Physics and Astrophysics*, WORLD SCIENTIFIC, 3rd ed. (2004), [10.1142/5024](#).
- [14] C. Giunti and C. Kim, *Fundamentals of Neutrino Physics and Astrophysics*, OUP Oxford (2007).
- [15] S.F. King, A. Merle, S. Morisi, Y. Shimizu and M. Tanimoto, *Neutrino Mass and Mixing: from Theory to Experiment*, *New J. Phys.* **16** (2014) 045018 [[arXiv:1402.4271](#)].
- [16] K. Zuber, *Neutrino physics*, Taylor & Francis (2020).
- [17] B. Dasgupta and J. Kopp, *Sterile Neutrinos*, *Phys. Rept.* **928** (2021) 1 [[arXiv:2106.05913](#)].
- [18] LSND collaboration, *Candidate events in a search for anti-muon-neutrino \rightarrow anti-electron-neutrino oscillations*, *Phys. Rev. Lett.* **75** (1995) 2650 [[nucl-ex/9504002](#)].
- [19] LSND collaboration, *Evidence for neutrino oscillations from the observation of $\bar{\nu}_e$ appearance in a $\bar{\nu}_\mu$ beam*, *Phys. Rev. D* **64** (2001) 112007 [[hep-ex/0104049](#)].

- [20] S. Gariazzo, C. Giunti, M. Laveder and Y.F. Li, *Model-independent $\bar{\nu}_e$ short-baseline oscillations from reactor spectral ratios*, *Phys. Lett. B* **782** (2018) 13 [[arXiv:1801.06467](#)].
- [21] MINIBOONE collaboration, *Significant Excess of ElectronLike Events in the MiniBooNE Short-Baseline Neutrino Experiment*, *Phys. Rev. Lett.* **121** (2018) 221801 [[arXiv:1805.12028](#)].
- [22] MINIBOONE COLLABORATION collaboration, *Updated miniboone neutrino oscillation results with increased data and new background studies*, *Phys. Rev. D* **103** (2021) 052002.
- [23] G. Mention, M. Fechner, T. Lasserre, T.A. Mueller, D. Lhuillier, M. Cribier et al., *The Reactor Antineutrino Anomaly*, *Phys. Rev. D* **83** (2011) 073006 [[arXiv:1101.2755](#)].
- [24] T.A. Mueller et al., *Improved Predictions of Reactor Antineutrino Spectra*, *Phys. Rev. C* **83** (2011) 054615 [[arXiv:1101.2663](#)].
- [25] P. Huber, *On the determination of anti-neutrino spectra from nuclear reactors*, *Phys. Rev. C* **84** (2011) 024617 [[arXiv:1106.0687](#)].
- [26] G.H. Collin, C.A. Argüelles, J.M. Conrad and M.H. Shaevitz, *First Constraints on the Complete Neutrino Mixing Matrix with a Sterile Neutrino*, *Phys. Rev. Lett.* **117** (2016) 221801 [[arXiv:1607.00011](#)].
- [27] S. Gariazzo, C. Giunti, M. Laveder and Y.F. Li, *Updated Global 3+1 Analysis of Short-BaseLine Neutrino Oscillations*, *JHEP* **06** (2017) 135 [[arXiv:1703.00860](#)].
- [28] A. Esmaili and A.Y. Smirnov, *Restricting the LSND and MiniBooNE sterile neutrinos with the IceCube atmospheric neutrino data*, *JHEP* **12** (2013) 014 [[arXiv:1307.6824](#)].
- [29] F. Capozzi, C. Giunti, M. Laveder and A. Palazzo, *Joint short- and long-baseline constraints on light sterile neutrinos*, *Phys. Rev. D* **95** (2017) 033006 [[arXiv:1612.07764](#)].
- [30] M. Dentler, A. Hernández-Cabezudo, J. Kopp, P.A.N. Machado, M. Maltoni, I. Martinez-Soler et al., *Updated Global Analysis of Neutrino Oscillations in the Presence of eV-Scale Sterile Neutrinos*, *JHEP* **08** (2018) 010 [[arXiv:1803.10661](#)].
- [31] MICROBOONE collaboration, *Search for an Excess of Electron Neutrino Interactions in MicroBooNE Using Multiple Final-State Topologies*, *Phys. Rev. Lett.* **128** (2022) 241801 [[arXiv:2110.14054](#)].
- [32] MICROBOONE collaboration, *First constraints on light sterile neutrino oscillations from combined appearance and disappearance searches with the MicroBooNE detector*, [arXiv:2210.10216](#).
- [33] C. Giunti, Y.F. Li, C.A. Ternes and Z. Xin, *Reactor antineutrino anomaly in light of recent flux model refinements*, *Phys. Lett. B* **829** (2022) 137054 [[arXiv:2110.06820](#)].
- [34] GALLEX collaboration, *First results from the Cr-51 neutrino source experiment with the GALLEX detector*, *Phys. Lett. B* **342** (1995) 440.
- [35] GALLEX collaboration, *GALLEX solar neutrino observations: Results for GALLEX IV*, *Phys. Lett. B* **447** (1999) 127.
- [36] F. Kaether, W. Hampel, G. Heusser, J. Kiko and T. Kirsten, *Reanalysis of the GALLEX solar neutrino flux and source experiments*, *Phys. Lett. B* **685** (2010) 47 [[arXiv:1001.2731](#)].
- [37] SAGE collaboration, *Measurement of the response of the Russian-American gallium experiment to neutrinos from a Cr-51 source*, *Phys. Rev. C* **59** (1999) 2246 [[hep-ph/9803418](#)].

- [38] SAGE collaboration, *Measurement of the solar neutrino capture rate by SAGE and implications for neutrino oscillations in vacuum*, *Phys. Rev. Lett.* **83** (1999) 4686 [[astro-ph/9907131](#)].
- [39] J.N. Abdurashitov et al., *Measurement of the response of a Ga solar neutrino experiment to neutrinos from an Ar-37 source*, *Phys. Rev. C* **73** (2006) 045805 [[nucl-ex/0512041](#)].
- [40] SAGE collaboration, *Measurement of the solar neutrino capture rate with gallium metal. III: Results for the 2002–2007 data-taking period*, *Phys. Rev. C* **80** (2009) 015807 [[arXiv:0901.2200](#)].
- [41] V.V. Barinov et al., *Results from the Baksan Experiment on Sterile Transitions (BEST)*, *Phys. Rev. Lett.* **128** (2022) 232501 [[arXiv:2109.11482](#)].
- [42] V.V. Barinov et al., *Search for electron-neutrino transitions to sterile states in the BEST experiment*, *Phys. Rev. C* **105** (2022) 065502 [[arXiv:2201.07364](#)].
- [43] C. Giunti, Y.F. Li, C.A. Ternes, O. Tyagi and Z. Xin, *Gallium Anomaly: Critical View from the Global Picture of ν_e and $\bar{\nu}_e$ Disappearance*, [arXiv:2209.00916](#).
- [44] C.A. Argüelles, T. Bertólez-Martínez and J. Salvado, *Impact of Wave Packet Separation in Low-Energy Sterile Neutrino Searches*, [arXiv:2201.05108](#).
- [45] T. Asaka, S. Blanchet and M. Shaposhnikov, *The nuMSM, dark matter and neutrino masses*, *Phys. Lett. B* **631** (2005) 151 [[hep-ph/0503065](#)].
- [46] T. Asaka and M. Shaposhnikov, *The ν MSM, dark matter and baryon asymmetry of the universe*, *Phys. Lett. B* **620** (2005) 17 [[hep-ph/0505013](#)].
- [47] A. Boyarsky, O. Ruchayskiy and M. Shaposhnikov, *The Role of sterile neutrinos in cosmology and astrophysics*, *Ann. Rev. Nucl. Part. Sci.* **59** (2009) 191 [[arXiv:0901.0011](#)].
- [48] M. Drewes et al., *A White Paper on keV Sterile Neutrino Dark Matter*, *JCAP* **01** (2017) 025 [[arXiv:1602.04816](#)].
- [49] R. Viollier, D. Trautmann and G. Tupper, *Supermassive neutrino stars and galactic nuclei*, *Physics Letters B* **306** (1993) 79.
- [50] N. Bilic, R.J. Lindebaum, G.B. Tupper and R.D. Viollier, *On the formation of degenerate heavy neutrino stars*, *Phys. Lett. B* **515** (2001) 105 [[astro-ph/0106209](#)].
- [51] P.C. de Holanda and A.Y. Smirnov, *Homestake result, sterile neutrinos and low-energy solar neutrino experiments*, *Phys. Rev. D* **69** (2004) 113002 [[hep-ph/0307266](#)].
- [52] P.C. de Holanda and A.Y. Smirnov, *Solar neutrino spectrum, sterile neutrinos and additional radiation in the Universe*, *Phys. Rev. D* **83** (2011) 113011 [[arXiv:1012.5627](#)].
- [53] P.S. Bhupal Dev and A. Pilaftsis, *Light and Superlight Sterile Neutrinos in the Minimal Radiative Inverse Seesaw Model*, *Phys. Rev. D* **87** (2013) 053007 [[arXiv:1212.3808](#)].
- [54] W. Liao, Y. Luo and X.-H. Wu, *Effect of interaction with neutrons in matter on flavor conversion of super-light sterile neutrino with active neutrino*, *JHEP* **06** (2014) 069 [[arXiv:1403.2559](#)].
- [55] P.C. Divari and J.D. Vergados, *Neutrino oscillations in the presence of super-light sterile neutrinos*, *Int. J. Mod. Phys. A* **31** (2016) 1650123 [[arXiv:1602.08690](#)].
- [56] SUPER-KAMIOKANDE collaboration, *Solar Neutrino Measurements in Super-Kamiokande-IV*, *Phys. Rev. D* **94** (2016) 052010 [[arXiv:1606.07538](#)].

- [57] SNO collaboration, *Combined Analysis of all Three Phases of Solar Neutrino Data from the Sudbury Neutrino Observatory*, *Phys. Rev. C* **88** (2013) 025501 [[arXiv:1109.0763](#)].
- [58] BOREXINO collaboration, *First Simultaneous Precision Spectroscopy of pp , ${}^7\text{Be}$, and pep Solar Neutrinos with Borexino Phase-II*, *Phys. Rev. D* **100** (2019) 082004 [[arXiv:1707.09279](#)].
- [59] A. de Gouvêa, G. Jusino Sánchez and K.J. Kelly, *Very light sterile neutrinos at NOvA and T2K*, *Phys. Rev. D* **106** (2022) 055025 [[arXiv:2204.09130](#)].
- [60] K.J. Kelly, P.A.N. Machado, S.J. Parke, Y.F. Perez-Gonzalez and R.Z. Funchal, *Neutrino mass ordering in light of recent data*, *Phys. Rev. D* **103** (2021) 013004 [[arXiv:2007.08526](#)].
- [61] M.A. Acero et al., *White Paper on Light Sterile Neutrino Searches and Related Phenomenology*, [arXiv:2203.07323](#).
- [62] Y.Y.Y. Wong, *Neutrino mass in cosmology: status and prospects*, *Ann. Rev. Nucl. Part. Sci.* **61** (2011) 69 [[arXiv:1111.1436](#)].
- [63] G. Franco Abellán, Z. Chacko, A. Dev, P. Du, V. Poulin and Y. Tsai, *Improved cosmological constraints on the neutrino mass and lifetime*, *JHEP* **08** (2022) 076 [[arXiv:2112.13862](#)].
- [64] T. Thakore, M.M. Devi, S. Kumar Agarwalla and A. Dighe, *Active-sterile neutrino oscillations at INO-ICAL over a wide mass-squared range*, *JHEP* **08** (2018) 022 [[arXiv:1804.09613](#)].
- [65] ICAL collaboration, *Physics Potential of the ICAL detector at the India-based Neutrino Observatory (INO)*, *Pramana* **88** (2017) 79 [[arXiv:1505.07380](#)].
- [66] R. Gandhi, B. Kayser, M. Masud and S. Prakash, *The impact of sterile neutrinos on CP measurements at long baselines*, *JHEP* **11** (2015) 039 [[arXiv:1508.06275](#)].
- [67] S. Choubey, D. Dutta and D. Pramanik, *Measuring the Sterile Neutrino CP Phase at DUNE and T2HK*, *Eur. Phys. J. C* **78** (2018) 339 [[arXiv:1711.07464](#)].
- [68] A. Dighe and S. Ray, *Signatures of heavy sterile neutrinos at long baseline experiments*, *Phys. Rev. D* **76** (2007) 113001 [[arXiv:0709.0383](#)].
- [69] S. Ray, *Neutrino oscillation phenomenology with fermions beyond the standard model*, Ph.D. thesis, Tata Inst., 2010.
- [70] N. Klop and A. Palazzo, *Imprints of CP violation induced by sterile neutrinos in T2K data*, *Phys. Rev. D* **91** (2015) 073017 [[arXiv:1412.7524](#)].
- [71] S.K. Agarwalla, S.S. Chatterjee and A. Palazzo, *Physics Reach of DUNE with a Light Sterile Neutrino*, *JHEP* **09** (2016) 016 [[arXiv:1603.03759](#)].
- [72] N. Haba, Y. Mimura and T. Yamada, *θ_{23} octant measurement in $3 + 1$ neutrino oscillations in T2HKK*, *Phys. Rev. D* **101** (2020) 075034 [[arXiv:1812.10940](#)].
- [73] K. Sharma and S. Patra, *Study of matter effects in the presence of sterile neutrino using OMSD approximation*, [arXiv:2207.03249](#).
- [74] Y. Kamo, S. Yajima, Y. Higashida, S.-I. Kubota, S. Tokuo and J.-I. Ichihara, *Analytical calculations of four neutrino oscillations in matter*, *Eur. Phys. J. C* **28** (2003) 211 [[hep-ph/0209097](#)].
- [75] W. Li, J. Ling, F. Xu and B. Yue, *Matter Effect of Light Sterile Neutrino: An Exact Analytical Approach*, *JHEP* **10** (2018) 021 [[arXiv:1808.03985](#)].

- [76] S.J. Parke and X. Zhang, *Compact Perturbative Expressions for Oscillations with Sterile Neutrinos in Matter*, *Phys. Rev. D* **101** (2020) 056005 [[arXiv:1905.01356](#)].
- [77] B. Yue, W. Li, J. Ling and F. Xu, *A compact analytical approximation for a light sterile neutrino oscillation in matter*, *Chin. Phys. C* **44** (2020) 103001 [[arXiv:1906.03781](#)].
- [78] Y. Reyimuaji and C. Liu, *Prospects of light sterile neutrino searches in long-baseline neutrino oscillations*, *JHEP* **06** (2020) 094 [[arXiv:1911.12524](#)].
- [79] C.S. Fong, *Analytic Neutrino Oscillation Probabilities*, [arXiv:2210.09436](#).
- [80] DUNE collaboration, *Long-Baseline Neutrino Facility (LBNF) and Deep Underground Neutrino Experiment (DUNE): Conceptual Design Report, Volume 2: The Physics Program for DUNE at LBNF*, [arXiv:1512.06148](#).
- [81] M. Lindner, T. Ohlsson and W. Winter, *A Combined treatment of neutrino decay and neutrino oscillations*, *Nucl. Phys. B* **607** (2001) 326 [[hep-ph/0103170](#)].
- [82] E.K. Akhmedov, R. Johansson, M. Lindner, T. Ohlsson and T. Schwetz, *Series expansions for three flavor neutrino oscillation probabilities in matter*, *JHEP* **04** (2004) 078 [[hep-ph/0402175](#)].
- [83] P. Huber, M. Lindner and W. Winter, *Simulation of long-baseline neutrino oscillation experiments with GLOBES (General Long Baseline Experiment Simulator)*, *Comput. Phys. Commun.* **167** (2005) 195 [[hep-ph/0407333](#)].
- [84] P. Huber, J. Kopp, M. Lindner, M. Rolinec and W. Winter, *New features in the simulation of neutrino oscillation experiments with GLOBES 3.0: General Long Baseline Experiment Simulator*, *Comput. Phys. Commun.* **177** (2007) 432 [[hep-ph/0701187](#)].
- [85] DUNE collaboration, *Prospects for beyond the Standard Model physics searches at the Deep Underground Neutrino Experiment*, *Eur. Phys. J. C* **81** (2021) 322 [[arXiv:2008.12769](#)].
- [86] MINOS+ collaboration, *Search for sterile neutrinos in MINOS and MINOS+ using a two-detector fit*, *Phys. Rev. Lett.* **122** (2019) 091803 [[arXiv:1710.06488](#)].